30th Anniversary of the Rencontres du Vietnam
Aug 6 – 12
ICISE
WINDOWS ON THE UNIVERSE
2023

Gravitational Waves from Early-Universe Turbulence: Detection Prospects through LISA and Stochastic Background Signal Observed by NANOGrav

Tina Kahniashvili
Carnegie Mellon University (USA)
Ilia State University (Georgia)

August 7 2023

Collaboration

- Axel Brandenburg
- Emma Clarke
- Grigol Gogoberidze
- Murman Gurgenidze
- Yutong He
- Arthur Kosowsky
- Andrew Long
- Sayan Mandal
- Deyan Mihaylov
- Matthias Rheinhardt
- Alberto Ropel Pol
- Jennifer Schober
- Nakul Shenoy
- Jonathan Stepp
- Guotong Sun

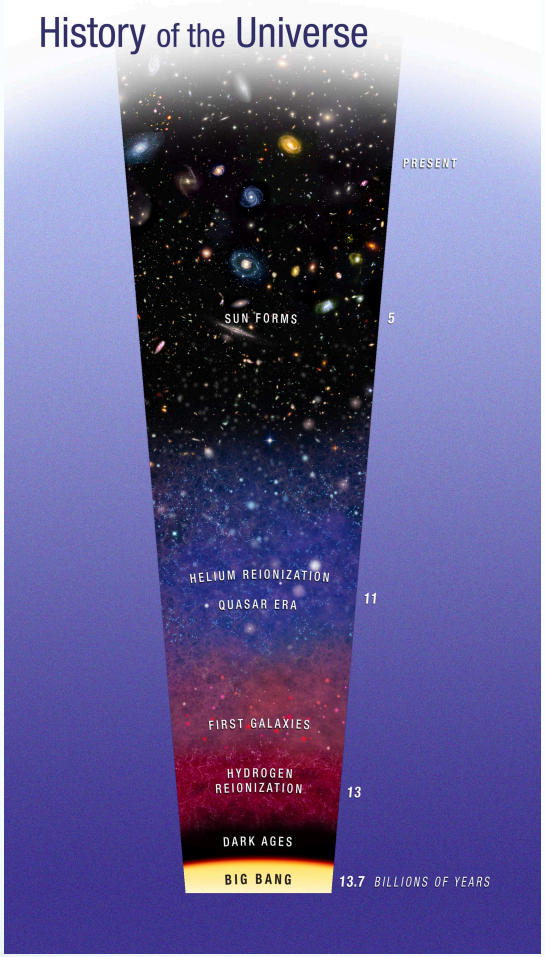
History of the Universe
PRESENT
SUN FORMS
5
HELIUM REIONIZATION
QUASAR ERA
11
FIRST GALAXIES
HYDROGEN REIONIZATION
13
DARK AGES
BIG BANG
13.7 BILLIONS OF YEARS

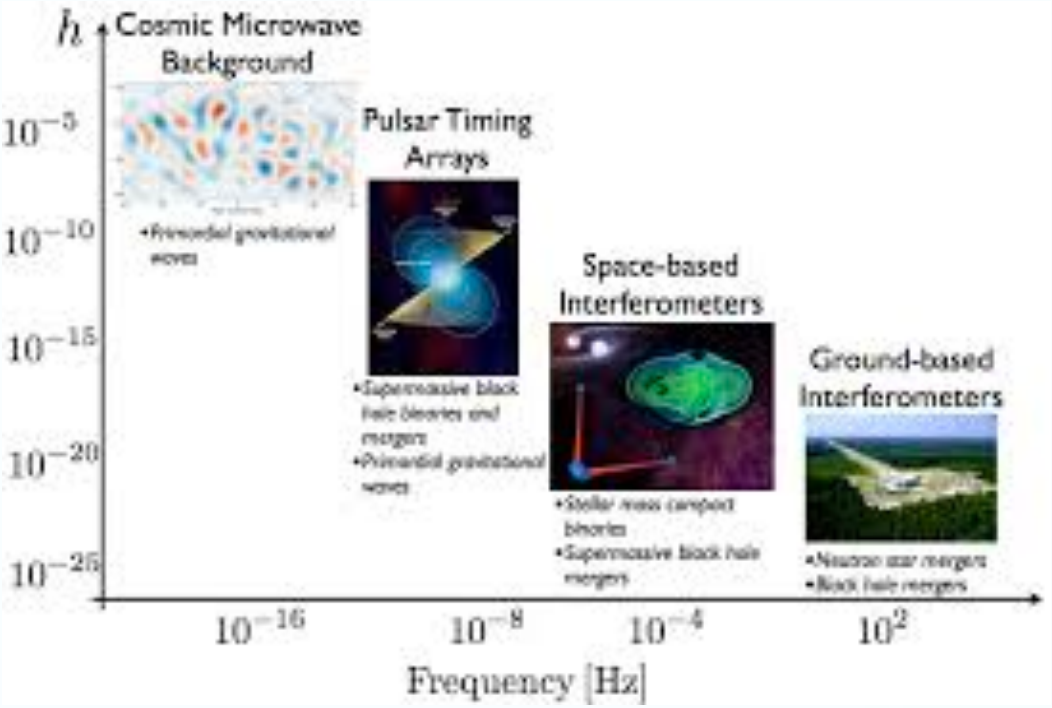
h
Cosmic Microwave Background
Pulsar Timing Arrays
Space-based Interferometers
Ground-based Interferometers
10^{-5}
10^{-10}
10^{-15}
10^{-20}
10^{-25}
10^{-16}
10^{-8}
10^{-4}
10^{2}
Frequency [Hz]

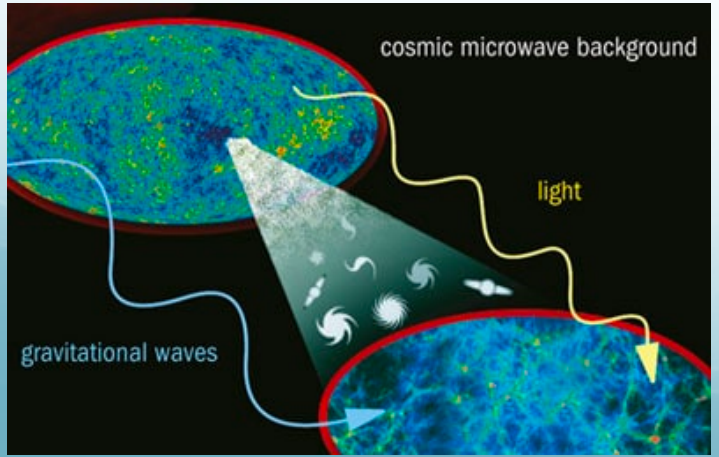
cosmic microwave background
light
gravitational waves

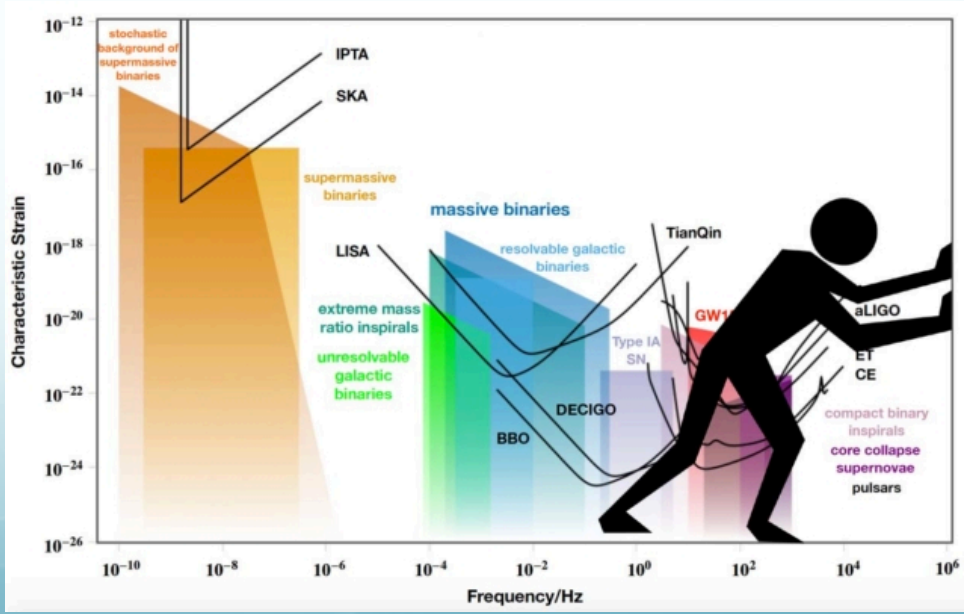
Characteristic Strain
Frequency/Hz
stochastic background of supermassive binaries
IPTA
SKA
supermassive binaries
massive binaries
LISA
resolvable galactic binaries
TianQin
extreme mass ratio inspirals
unresolvable galactic binaries
Type IA SN
GW1
aLIGO
ET
CE
DECIGO
BBO
compact binary inspirals
core collapse supernovae
pulsars

Living Rev Relativ (2017) 20:2
https://doi.org/10.1007/s41114-017-0004-1

REVIEW ARTICLE

Detection methods for stochastic gravitational-wave backgrounds: a unified treatment

Joseph D. Romano[1] · **Neil. J. Cornish**[2]

A cosmological background produced by the superposition of a large number of independent gravitational-wave signals from the early Universe is expected to be Gaussian (via the central limit theorem), as well as isotropically-distributed on the sky. Contrast this with the superposition of gravitational waves produced by unresolved Galactic white-dwarf binaries radiating in the LISA band (10^{-4} Hz to 10^{-1} Hz). Although this confusion-limited astrophysical foreground is also expected to be Gaussian and stationary, it will have an anisotropic distribution, following the spatial distribution of the Milky Way. The anistropy will be encoded as amodulation in the LISA output, due to the changing antenna pattern of the LISA constellation in its yearly orbit around the Sun.

Gravitational Waves from Phase Transitions

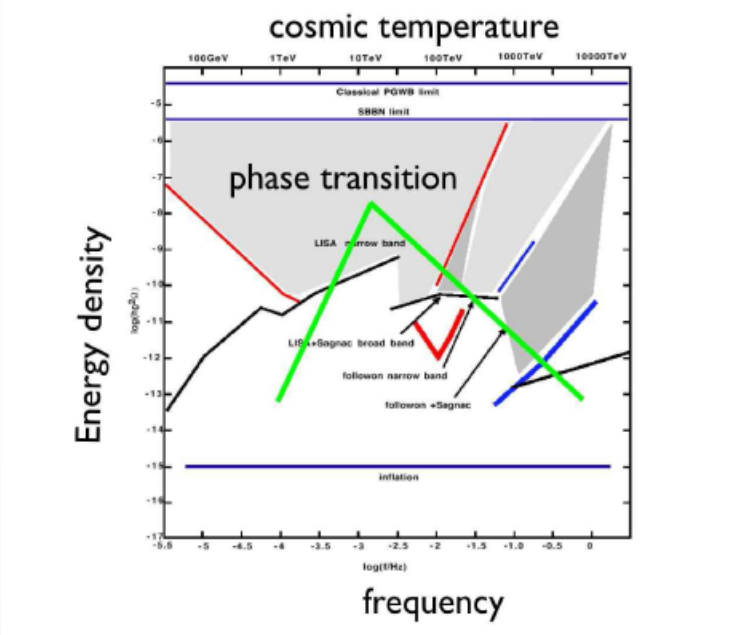

Pioneering works:

- Winicour 1973
- Hogan 1982, 1986
- Turner & Wilczek 1990
- Kosowsky, Turner, Watkins. 1992
- Kosowsky & Turner 1993
- Kamionkowski et al. 1994

C. Hogan, 2006

First order phase transitions?

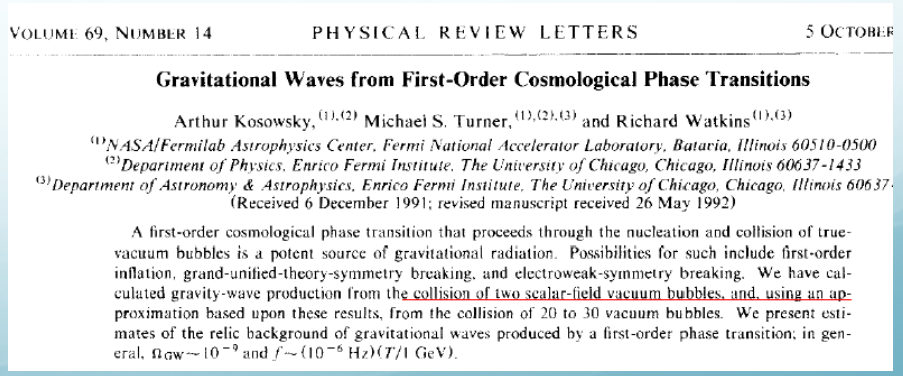

VOLUME 69, NUMBER 14 PHYSICAL REVIEW LETTERS 5 OCTOBER

Gravitational Waves from First-Order Cosmological Phase Transitions

Arthur Kosowsky,[1,2] Michael S. Turner,[1,2,3] and Richard Watkins[1,3]

[1]*NASA/Fermilab Astrophysics Center, Fermi National Accelerator Laboratory, Batavia, Illinois 60510-0500*

[2]*Department of Physics, Enrico Fermi Institute, The University of Chicago, Chicago, Illinois 60637-1433*

[3]*Department of Astronomy & Astrophysics, Enrico Fermi Institute, The University of Chicago, Chicago, Illinois 60637*

(Received 6 December 1991; revised manuscript received 26 May 1992)

A first-order cosmological phase transition that proceeds through the nucleation and collision of true-vacuum bubbles is a potent source of gravitational radiation. Possibilities for such include first-order inflation, grand-unified-theory-symmetry breaking, and electroweak-symmetry breaking. We have calculated gravity-wave production from the collision of two scalar-field vacuum bubbles, and, using an approximation based upon these results, from the collision of 20 to 30 vacuum bubbles. We present estimates of the relic background of gravitational waves produced by a first-order phase transition; in general, $\Omega_{GW} \sim 10^{-9}$ and $f \sim (10^{-6}\ \mathrm{Hz})(T/1\ \mathrm{GeV})$.

Turbulence

Atmospheric science

marine science

aerodynamics

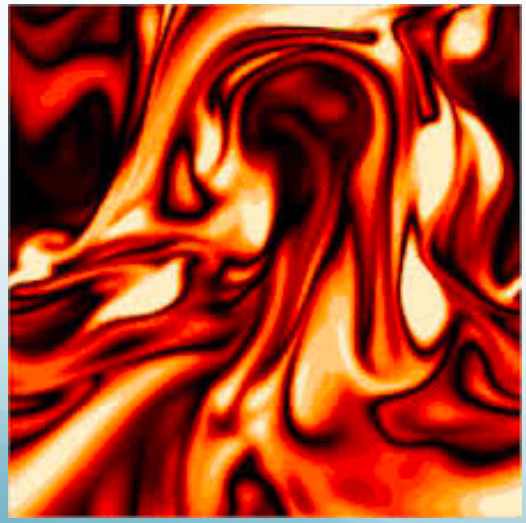

Astrophysical plasma

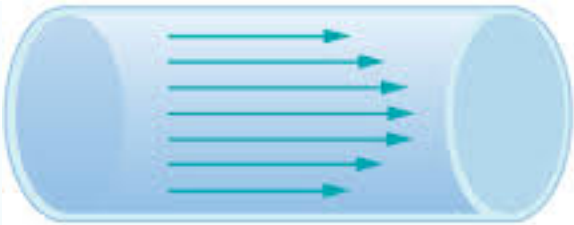

(a) Laminar Flow

(b) Turbulent Flow

Possible Sources

- Cosmological Phase Transitions

Bubbles collisions and nucleation

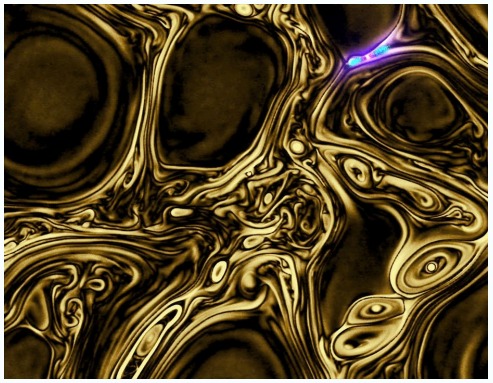

Baym et al. 1995

- Primordial Magnetic Fields

Quashnock, et al. 1989

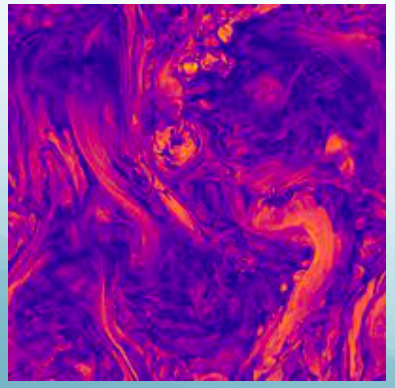

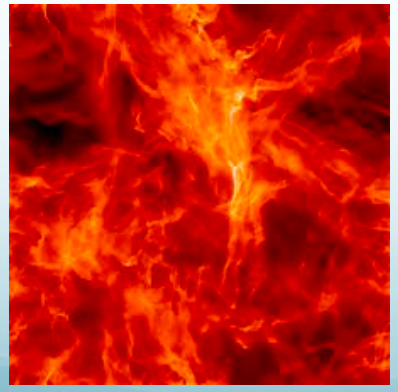

Galishnikova et al. 2022

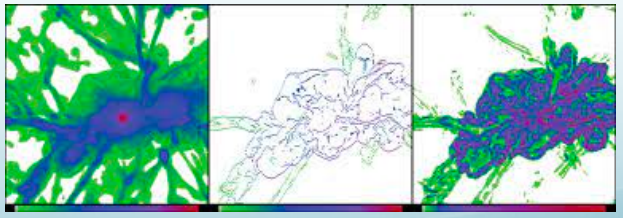

Ryu et al. 2020

Modeling Primordial Turbulence

- primordial plasma is perfect conductor
- interaction between primordial magnetic fields and fluid (plasma)
- development of turbulence and vs. generation of magnetic fields

$$\frac{\partial \rho}{\partial t} + \nabla \cdot [\rho \mathbf{v}] = 0$$

$$\frac{\partial (\rho \mathbf{v})}{\partial t} + \nabla \cdot [\rho \mathbf{v}\mathbf{v} - \mathbf{B}\mathbf{B} + \mathsf{P}^*] = 0$$

$$\frac{\partial E}{\partial t} + \nabla \cdot [(E + P^*)\mathbf{v} - \mathbf{B}\,(\mathbf{B} \cdot \mathbf{v})] = 0$$

$$\frac{\partial \mathbf{B}}{\partial t} - \nabla \times (\mathbf{v} \times \mathbf{B}) = 0$$

$$P^* = P + \frac{\mathbf{B} \cdot \mathbf{B}}{2}$$

$$E = P/(\gamma - 1) + \frac{\rho(\mathbf{v} \cdot \mathbf{v})}{2} + \frac{\mathbf{B} \cdot \mathbf{B}}{2}$$

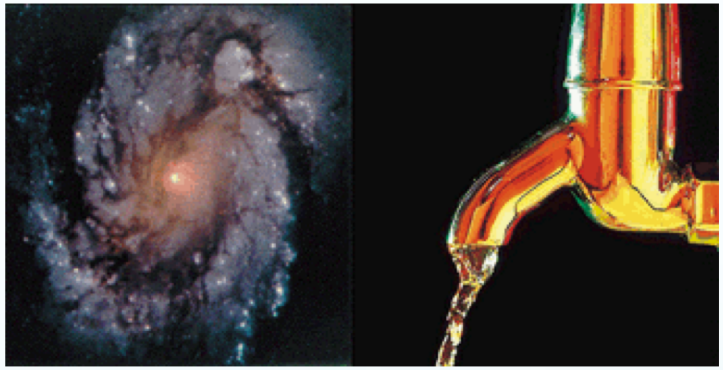

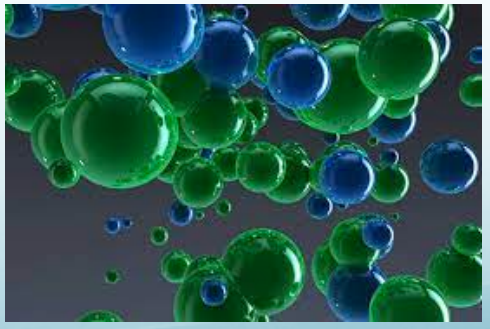

Penders, Jones, Porter, 2019

Primordial Magnetic Fields and Turbulence Gravitational Waves

Mon. Not. R. astr. Soc. (1987) **229**, 357–370

$$\nabla^2 h_{ij}(\boldsymbol{x},t) - \frac{\partial^2}{\partial t^2} h_{ij}(\boldsymbol{x},t) = -16\pi G\, S_{ij}(\boldsymbol{x},t)$$

Generation of gravitational waves by the anisotropic phases in the early Universe

D. V. Deryagin, D. Yu. Grigoriev and V. A. Rubakov *Institute for Nuclear Research, USSR Academy of Sciences, Moscow 117312, USSR*

M. V. Sazhin *P. K. Sternberg Astronomical Institute, Universitetskii pr. 13, Moscow 119899, USSR*

The space interferometer will be a unique device to observe the gravitational radiation from anisotropic phases possible at the energy scales 1TeV-100GeV.

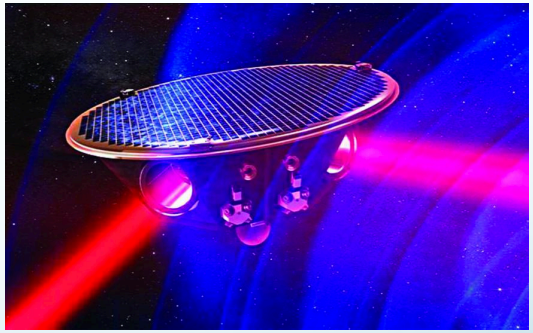

Pulsar Timing Array (PTA) are sensible to gravitational waves generated or present at QCD energy scales

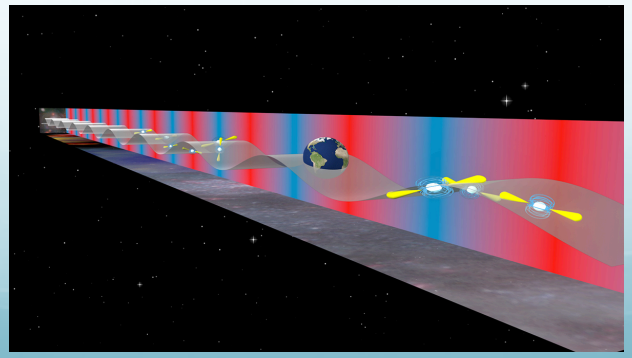

Waves from Turbulence

$$\nabla \delta\rho\,(\mathbf{x},t) - \frac{1}{c_s^2}\frac{\partial^2}{\partial t^2}\,\delta\rho\,(\mathbf{x},t) = -\frac{\partial^2}{\partial x^i \partial x^j}\,T_{ij}\,(\mathbf{x},t), \qquad c_s^2 = \frac{\partial p}{\partial \rho}$$

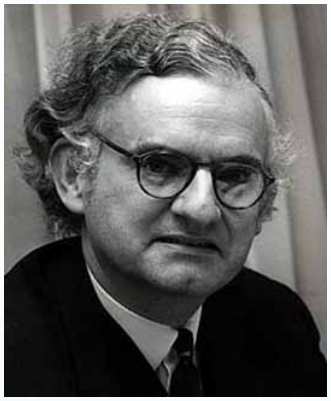

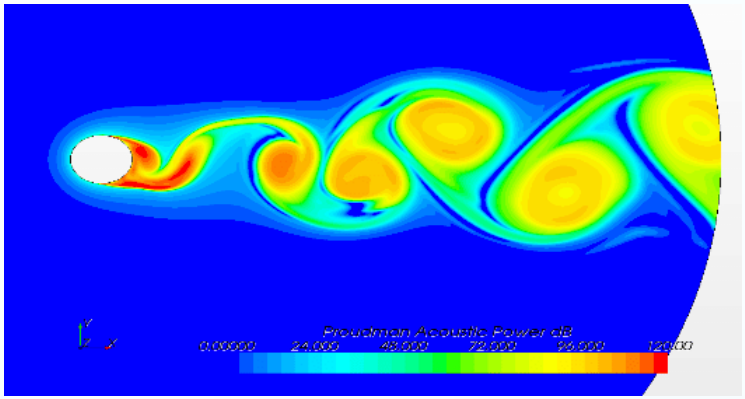

Lighthill, 1952;
Proudman 1952

$$c = 1$$

$$\nabla^2 h_{ij}(\boldsymbol{x},t) - \frac{\partial^2}{\partial t^2} h_{ij}(\boldsymbol{x},t) = -16\pi G\, S_{ij}(\boldsymbol{x},t)$$

What is the difference?

Gravitational Waves from Turbulence

$$\nabla^2 h_{ij}(\boldsymbol{x},t) - \frac{\partial^2}{\partial t^2} h_{ij}(\boldsymbol{x},t) = -16\pi G\, S_{ij}(\boldsymbol{x},t)$$

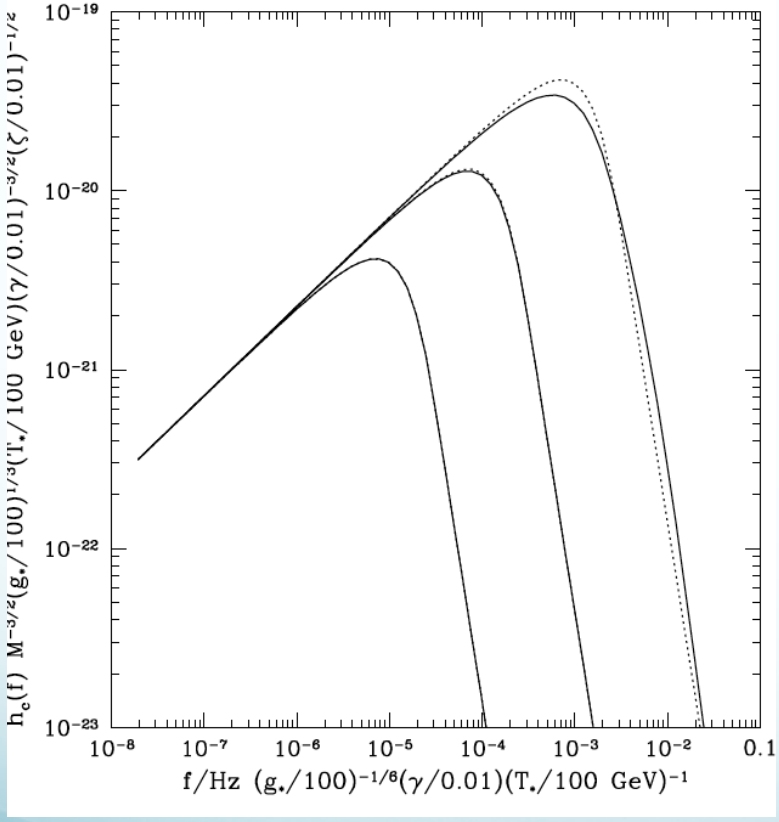

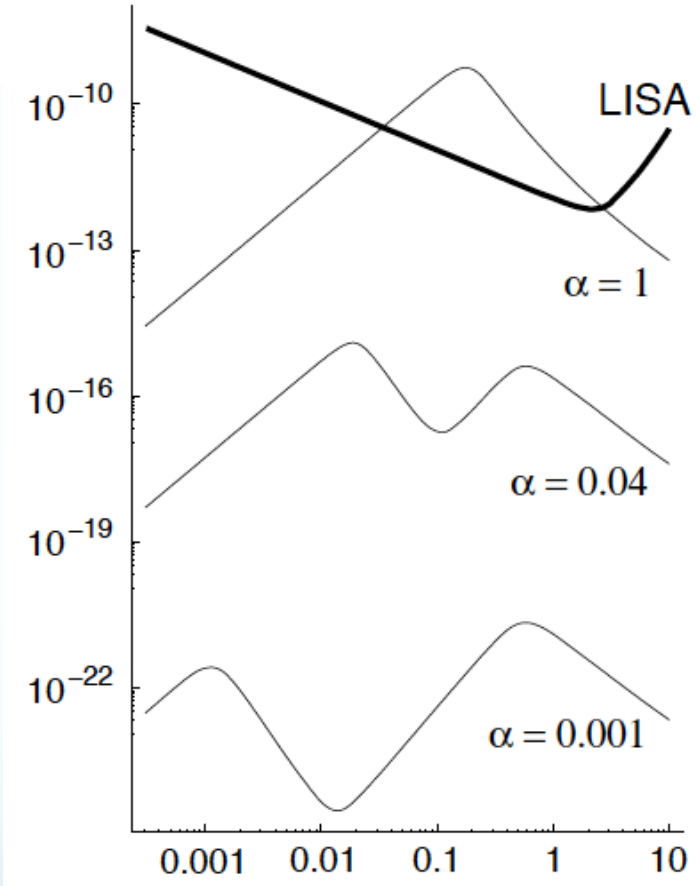

Nicolis 2004

Gogoberidze, et al. 2007

$$h_{ij}(\boldsymbol{x},t) = 4G \int d^3\boldsymbol{x}' \frac{S_{ij}(\boldsymbol{x}',\ t - |\boldsymbol{x}-\boldsymbol{x}'|)}{|\boldsymbol{x}-\boldsymbol{x}'|}$$

Numerical Simulations

- To account properly non-linear processes (MHD)
- Not be limited by the short duration of the phase transitions
- Three stages turbulence decay
  - Forced turbulence
  - Stationary turbulence
  - Free decay
- The decaying source is present till recombination (after the field is frozen in)
- Results – strongly initial conditions dependent
- It is assumed the stationary turbulence while in reality turbulence decays

$$\left(\frac{\partial^2}{\partial t^2} - c^2\nabla^2\right) h_{ij}^{\mathrm{TT}} = \frac{16\pi G}{a^3 c^2} T_{ij}^{\mathrm{TT}}$$

$$h_{ij}^{\mathrm{TT}} = a h_{ij}^{\mathrm{TT,phys}} \qquad \mathrm{d}t_{\mathrm{phys}} = a\mathrm{d}t$$

Grishchuk 1974

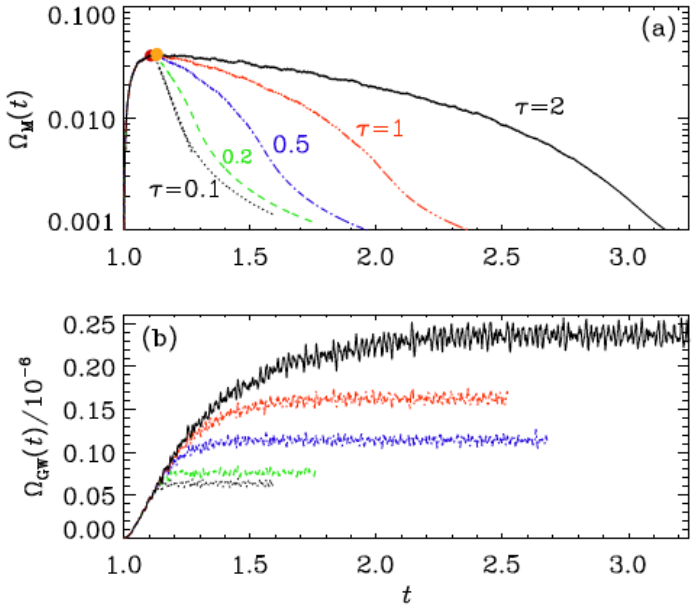

FIG. 1: Evolution of magnetic energy (top) and growth of GW energy density (bottom) for simulations where the driving is turned off at $t = 1.1$ (black dotted line), or the strength of the driving is reduced linearly in time over the duration $\tau = 0.2$ (green), 0.5 (blue), 1 (red), or 2 (black). Time is in units of the Hubble time at the moment of source activation.

Roper Pol et al. 2019

Kahniashvili et al. 2021

Three Stages of Generation

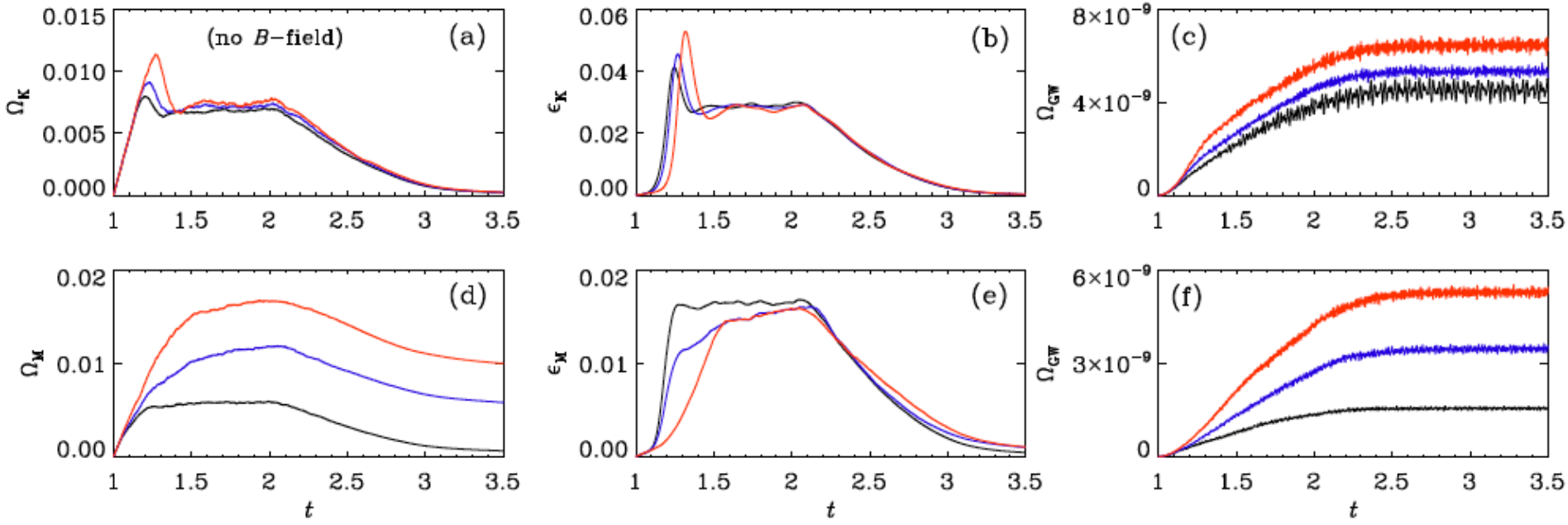

FIG. 2: Evolution of (a) Ω_K, (b) ϵ_K, and (c) Ω_{GW} for kinetically driven cases with $\sigma = 0$ (black), 0.5 (blue), and 1 (red), and of (d) Ω_M, (e) ϵ_M, and (f) Ω_{GW} for magnetically driven cases with $\sigma = 0$ (black), 0.3 (blue), and 1 (red).

Kahniashvili et al. 2020

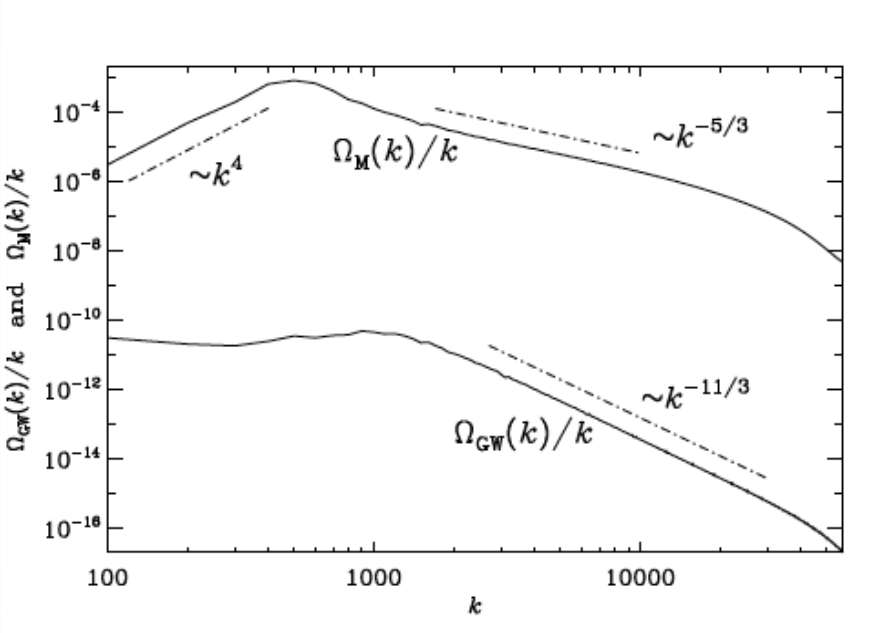

Magnetic and GW energy spectra averaged over late times (t > 1.1), after the GW spectrum has started to fluctuate around a steady state.

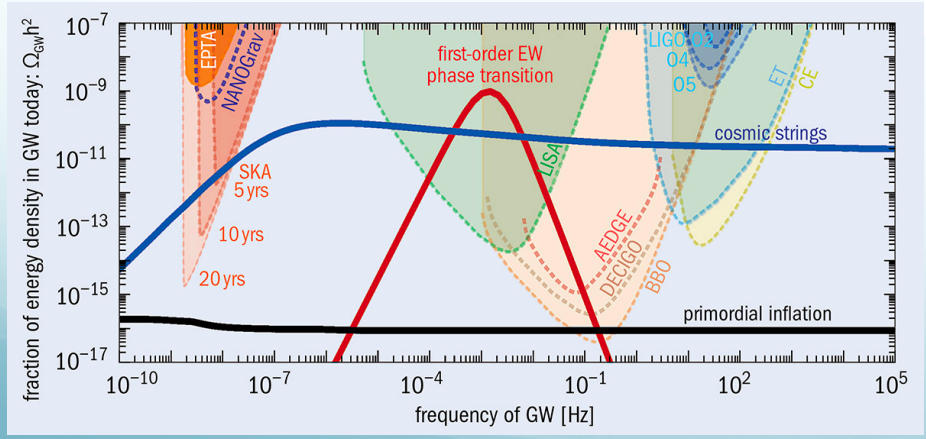

LISA Cosmology Group

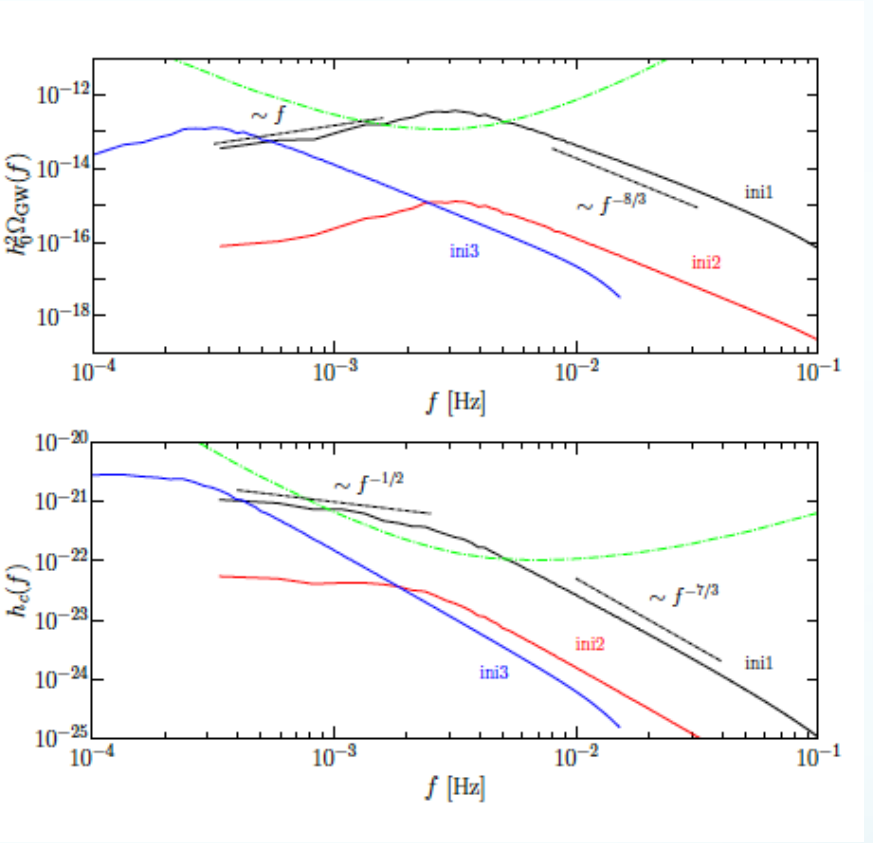

Spectra of $h_0^2\ \Omega_{GW}(f)$ and $h_c(f)$ evaluated at the present time, along with the LISA sensitivity curve (green dot-dashed line) to a stochastic GW background after four years of mission.

Roper Pol et al. 2019

Pulsar Timing Arrays: nanoGrav

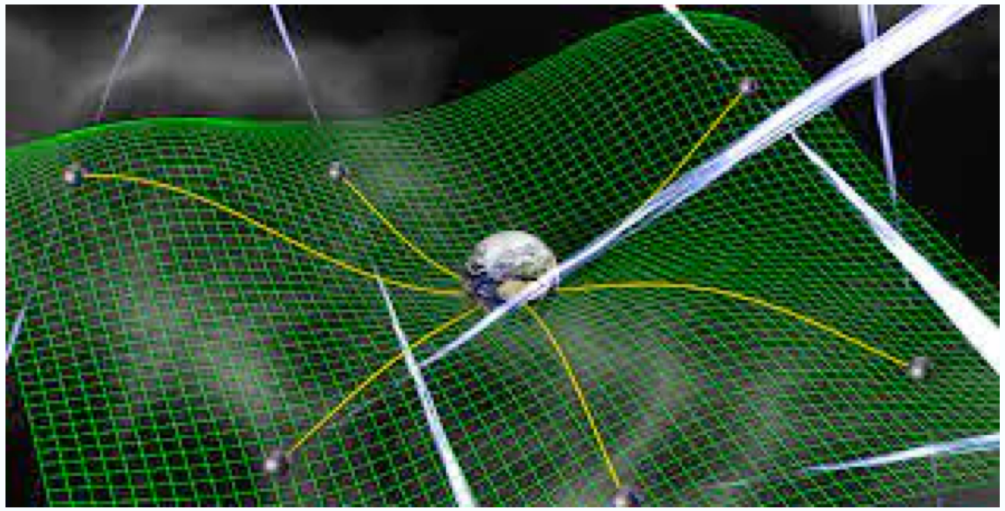

$$h_c(f) = A_{\rm CP}\left(\frac{f}{f_{\rm yr}}\right)^{\alpha_{\rm CP}},$$

$$\Omega_{\rm GW}(t,f) = \frac{1}{\mathcal{E}_{\rm crit}(t)}\frac{{\rm d}\mathcal{E}_{\rm GW}}{{\rm dln}f}$$

NANOGrav 12.5-year sensitivity range of 1–100 nHz

$$\Omega_{\rm GW}(f) = \frac{2\pi^2}{3H_0^2}f^2h_c^2(f) = \Omega_{\rm GW}^{\rm yr}\left(\frac{f}{f_{\rm yr}}\right)^{5-\gamma_{\rm CP}}$$

Arzoumanian et al (2021)

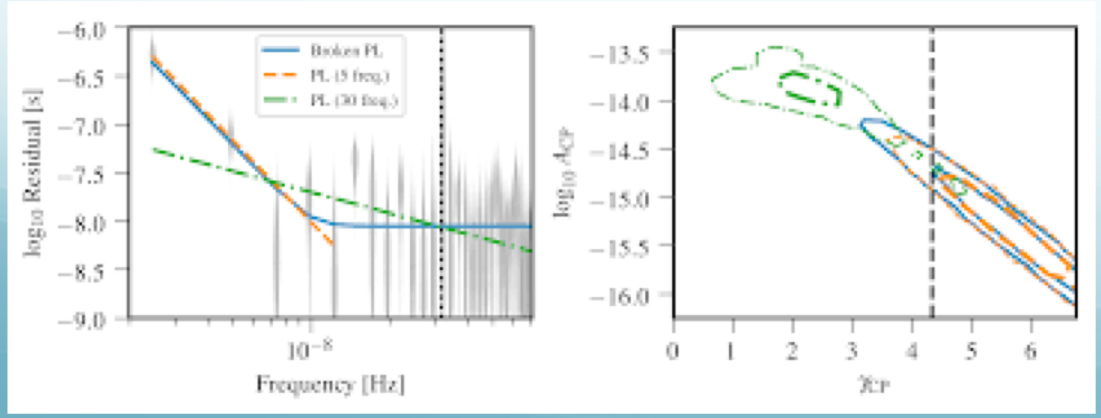

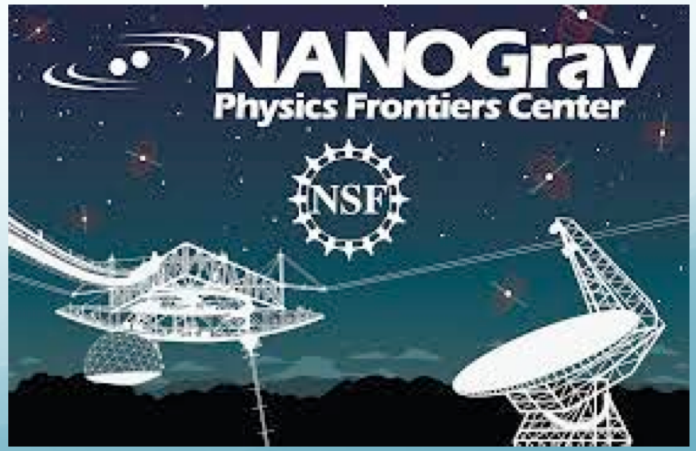

Astrophysical:

✓ Super massive black hole binary (SMBHB) (Phinney 2001): γ=13/3

Cosmological:

✓ Bubbles collisions (Kosowsky et. Al. 1993)
✓ Inflation (Vagnozzi 2020)
✓ Cosmic strings (Blanco-Pillado et al. 2020)
✓ Seed magnetic fields and MHD Turbulence (Neronov et. al. 2020)
✓ Hydrodynamic and MHD Turbulence (Brandenburg et al. 2021)

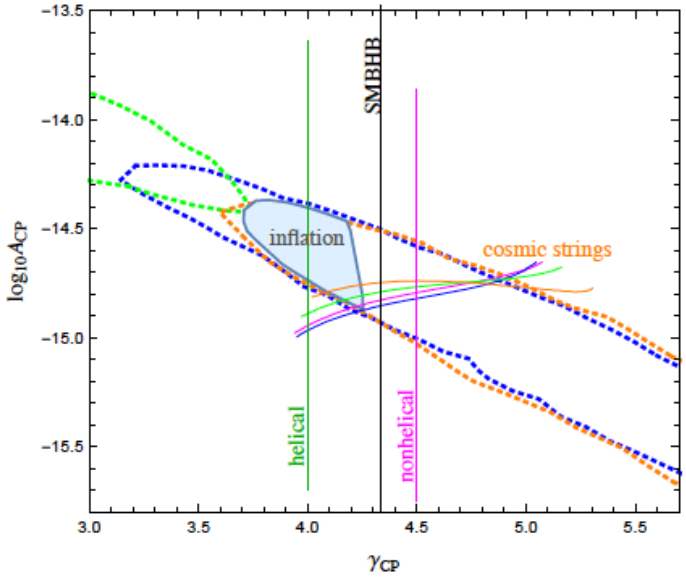

Credit: Emma Clarke

QCD energy scale

$$\frac{a_0}{a_\star} = 10^{12}\left(\frac{g_{S,\star}}{15}\right)^{\frac{1}{3}}\left(\frac{T_\star}{150\ \mathrm{MeV}}\right)$$

$$H_\star^2 = \frac{8\pi G}{2}\mathcal{E}_{\mathrm{rad},\star} \qquad \mathcal{E}_{\mathrm{rad},\star} = \frac{\pi^2 g_\star}{30}T_\star^4 \qquad (c = k_B = \hbar = 1)$$

$$f_H \simeq (1.8\times10^{-8}\mathrm{Hz})10^{12}\left(\frac{g_\star}{15}\right)^{\frac{1}{3}}\left(\frac{T_\star}{150\ \mathrm{MeV}}\right)$$

NanoGrav & Phase Transitions

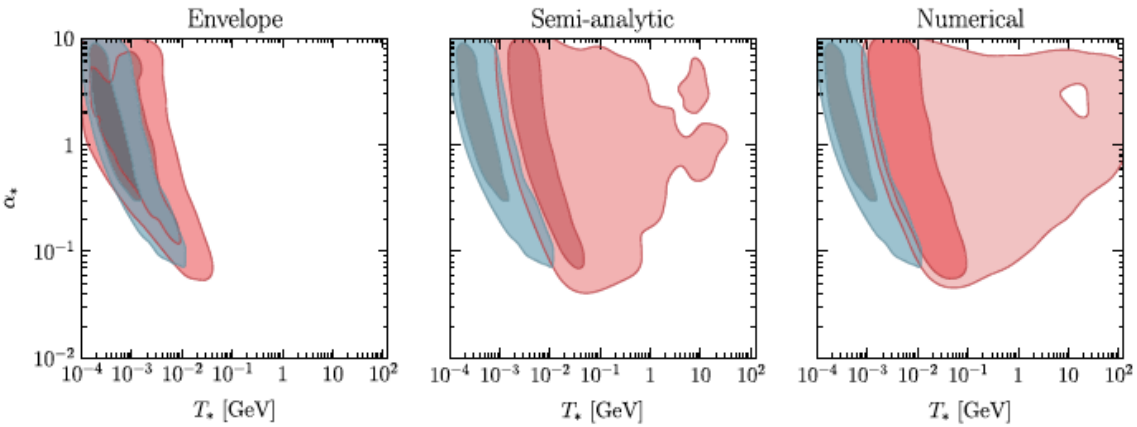

FIG. 1. In red (blue) the 1-σ (68% posterior credible level), and 2-σ (95% posterior credible level) contours for the two-dimensional posterior distributions in the (T_*, α_*) plane obtained in the BO (SWO). The BO analysis has been performed with the spectral shape computed by using the envelope approximation (left panel), semianalytic results (central panel), and numerical results (right panel). Specifically, we use $(a, b, c) = (1, 2.61, 1.5)$ for the semianalytic results, and $(a, b, c) = (0.7, 2.3, 1)$ for the numerical results.

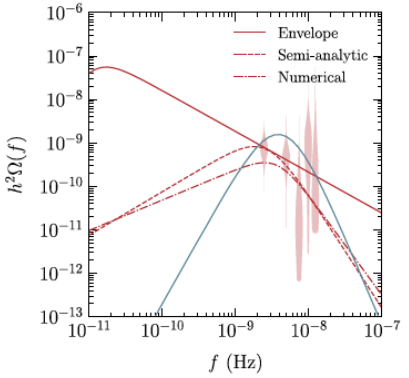

FIG. 2. Maximum likelihood GWB fractional energy-density spectrum for the BO (red) and SWO (blue) analyses compared with the marginalized posterior for the free power spectrum (independent per-frequency characterization; red violin plot) derived in NG12gwb For the BO analysis we show the results derived by using the envelope (solid line), semianalytic (dashed), and numerical (dot-dashed) spectral shapes. For the BO analyses the values of (α_*, T_*) for these maximum likelihood spectra are (0.28,0.7 MeV) for the envelope results, (1.2,3.4 MeV) for the semianalytic results, and (0.13,14.1 MeV) for the numerical results. While for the SO analysis we get (6.0,0.32 MeV).

TABLE I. Parameters for the gravitational wave spectrum of Eq. (4). The values of the parameters (a, b, c) in the spectral shape of the bubble contribution are reported in Table II.

	Bubbles [58]	Sound waves [59]
$\Delta(v_w)$	$[0.48 v_w^3/(1+5.3 v_w^2+5 v_w^4)]$	$0.513 v_w$
κ	κ_ϕ	$\kappa_{\rm SW}$
p	2	2
q	2	1
$\mathcal{S}(x)$	$\{(a+b)^c/[b x^{-a/c}+a x^{b/c}]^c\}$	$x^3[7/(4+3x^2)]^{7/2}$
f_*/β	$[0.35/(1+0.07 v_w+0.69 v_w^4)]$	$(0.536/v_w)$

T_* [GeV]	Phase transition temperature
α_*	Phase transition strength
H_*/β	Bubble nucleation rate
v_w	Bubble wall velocity

PHYSICAL REVIEW LETTERS **127,** 251302 (2021)

Editors' Suggestion | Featured in Physics

Searching for Gravitational Waves from Cosmological Phase Transitions with the NANOGrav 12.5-Year Dataset

Zaven Arzoumanian,[1] Paul T. Baker,[2] Harsha Blumer,[3,4] Bence Bécsy,[5] Adam Brazier,[6,7] Paul R. Brook,[3,4] Sarah Burke-Spolaor,[3,4,8] Maria Charisi,[9] Shami Chatterjee,[6] Siyuan Chen,[10,11,12] James M. Cordes,[6] Neil J. Cornish,[5] Fronefield Crawford,[13] H. Thankful Cromartie,[6] Megan E. DeCesar,[14,15*] Paul B. Demorest,[16] Timothy Dolch,[17,18] Justin A. Ellis,[19] Elizabeth C. Ferrara,[20,21,22] William Fiore,[3,4] Emmanuel Fonseca,[23] Nathan Garver-Daniels,[3,4] Peter A. Gentile,[3,4] Deborah C. Good,[24] Jeffrey S. Hazboun,[25] A. Miguel Holgado,[26,27] Kristina Islo,[28] Ross J. Jennings,[6] Megan L. Jones,[28] Andrew R. Kaiser,[3,4] David L. Kaplan,[28] Luke Zoltan Kelley,[29] Joey Shapiro Key,[25] Nima Laal,[30] Michael T. Lam,[31,32] T. Joseph W. Lazio,[33] Vincent S. H. Lee,[34] Duncan R. Lorimer,[3,4] Jing Luo,[35] Ryan S. Lynch,[36] Dustin R. Madison,[3,4] Maura A. McLaughlin,[3,4] Chiara M. F. Mingarelli,[37,38] Andrea Mitridate,[34] Cherry Ng,[39] David J. Nice,[14] Timothy T. Pennucci,[40,41] Nihan S. Pol,[3,4,9] Scott M. Ransom,[40] Paul S. Ray,[42] Brent J. Shapiro-Albert,[3,4] Xavier Siemens,[30,28] Joseph Simon,[33,43] Renée Spiewak,[44] Ingrid H. Stairs,[24] Daniel R. Stinebring,[45] Kevin Stovall,[16] Jerry P. Sun,[30] Joseph K. Swiggum,[14] Stephen R. Taylor,[9] Jacob E. Turner,[3,4] Michele Vallisneri,[33] Sarah J. Vigeland,[28] Caitlin A. Witt,[3,4] and Kathryn M. Zurek[34]

(NANOGrav Collaboration)

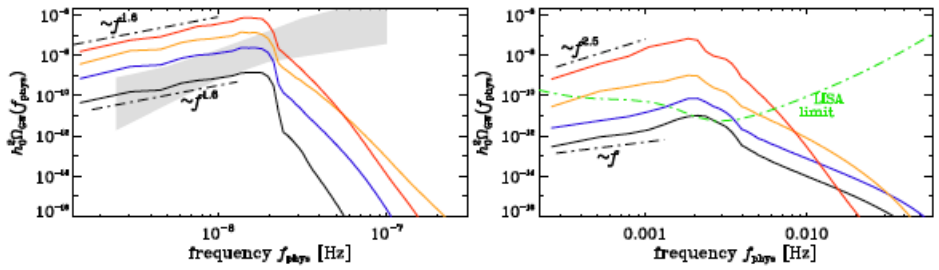

FIG. 2: Frequency spectra, $h_0^2\Omega_{\rm GW}(f)$, for both the QCDPT Runs a–d (left) and the EWPT Runs A–D (right) shown in red, orange, blue, and black, respectively.

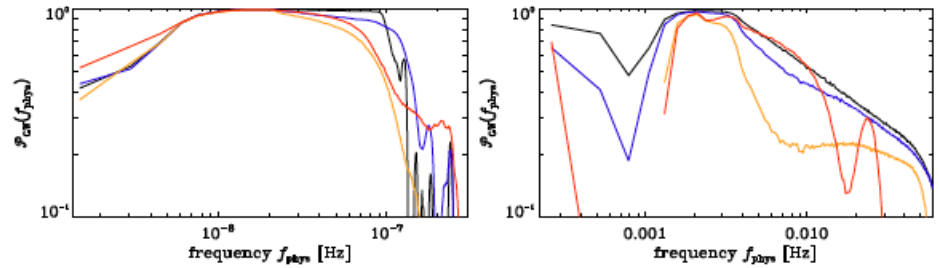

FIG. 3: Polarization spectra, $\mathcal{P}_{\rm GW}(f)$, for the QCDPT Runs a–d (left) and the EWPT Runs A–D (right) [56] shown in red, orange, blue, and black, respectively.

Kahniashvili et al. 2021

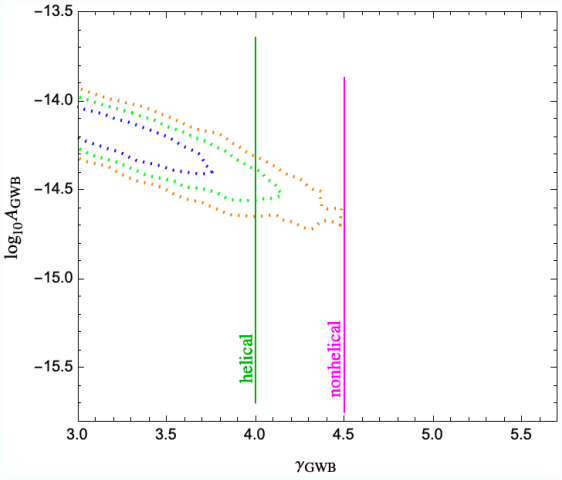

Credit: Emma Clarke

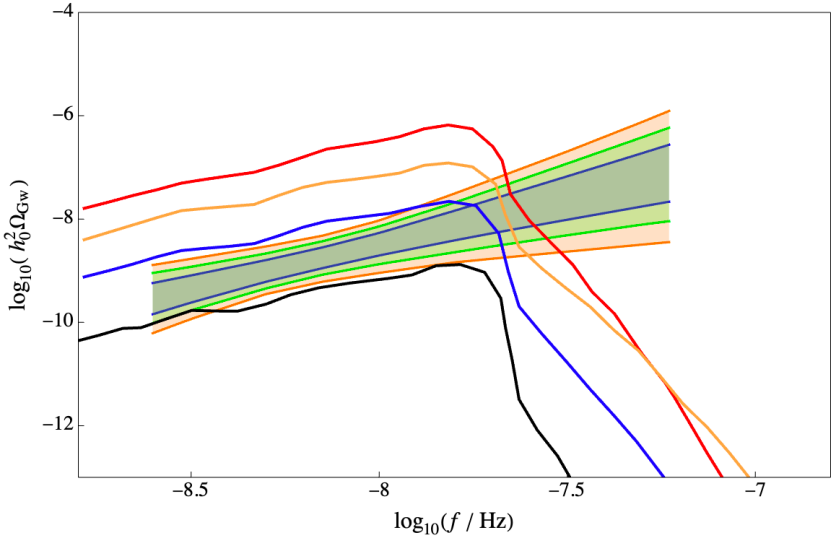

The Astrophysical Journal Letters, 951:L8 (24pp), 2023 July 1 https://doi.org/10.3847/2041-8213/acdac6

The NANOGrav 15 yr Data Set: Evidence for a Gravitational-wave Background

Gabriella Agazie[1], Akash Anumarlapudi[1], Anne M. Archibald[2], Zaven Arzoumanian[3], Paul T. Baker[4], Bence Bécsy[5], Laura Blecha[6], Adam Brazier[7,8], Paul R. Brook[9], Sarah Burke-Spolaor[10,11], Rand Burnette[5], Robin Case[5], Maria Charisi[12], Shami Chatterjee[7], Katerina Chatziioannou[13], Belinda D. Cheeseboro[10,11], Siyuan Chen[14], Tyler Cohen[15], James M. Cordes[7], Neil J. Cornish[16], Fronefield Crawford[17], H. Thankful Cromartie[7,70], Kathryn Crowter[18], Curt J. Cutler[13,19], Megan E. DeCesar[20], Dallas DeGan[5], Paul B. Demorest[21], Heling Deng[5], Timothy Dolch[22,23], Brendan Drachler[24,25], Justin A. Ellis[26], Elizabeth C. Ferrara[27,28,29], William Fiore[10,11], Emmanuel Fonseca[10,11], Gabriel E. Freedman[1], Nate Garver-Daniels[10,11], Peter A. Gentile[10,11], Kyle A. Gersbach[12], Joseph Glaser[10,11], Deborah C. Good[30,31], Kayhan Gültekin[32], Jeffrey S. Hazboun[5], Sophie Hourihane[13], Kristina Islo[1], Ross J. Jennings[10,11,73], Aaron D. Johnson[1,13], Megan L. Jones[1], Andrew R. Kaiser[10,11], David L. Kaplan[1], Luke Zoltan Kelley[33], Matthew Kerr[34], Joey S. Key[35], Tonia C. Klein[1], Nima Laal[5], Michael T. Lam[24,25], William G. Lamb[12], T. Joseph W. Lazio[19], Natalia Lewandowska[36], Tyson B. Littenberg[37], Tingting Liu[10,11], Andrea Lommen[38], Duncan R. Lorimer[10,11], Jing Luo[39,71], Ryan S. Lynch[40], Chung-Pei Ma[33,41], Dustin R. Madison[42], Margaret A. Mattson[10,11], Alexander McEwen[1], James W. McKee[43,44], Maura A. McLaughlin[10,11], Natasha McMann[12], Bradley W. Meyers[18,45], Patrick M. Meyers[13], Chiara M. F. Mingarelli[30,31,46], Andrea Mitridate[47], Priyamvada Natarajan[48,49], Cherry Ng[50], David J. Nice[51], Stella Koch Ocker[7], Ken D. Olum[52], Timothy T. Pennucci[53], Benetge B. P. Perera[54], Polina Petrov[12], Nihan S. Pol[12], Henri A. Radovan[55], Scott M. Ransom[56], Paul S. Ray[34], Joseph D. Romano[57], Shashwat C. Sardesai[1], Ann Schmiedekamp[58], Carl Schmiedekamp[58], Kai Schmitz[59], Levi Schult[12], Brent J. Shapiro-Albert[10,11,60], Xavier Siemens[1,5], Joseph Simon[61,72], Magdalena S. Siwek[62], Ingrid H. Stairs[18], Daniel R. Stinebring[63], Kevin Stovall[21], Jerry P. Sun[5], Abhimanyu Susobhanan[1], Joseph K. Swiggum[51,72], Jacob Taylor[5], Stephen R. Taylor[12], Jacob E. Turner[10,11], Caner Unal[64,65], Michele Vallisneri[13,19], Rutger van Haasteren[66], Sarah J. Vigeland[1], Haley M. Wahl[10,11], Qiaohong Wang[12], Caitlin A. Witt[67,68], and Olivia Young[24,25]
The NANOGrav Collaboration[69]

Gravitational Waves Missions

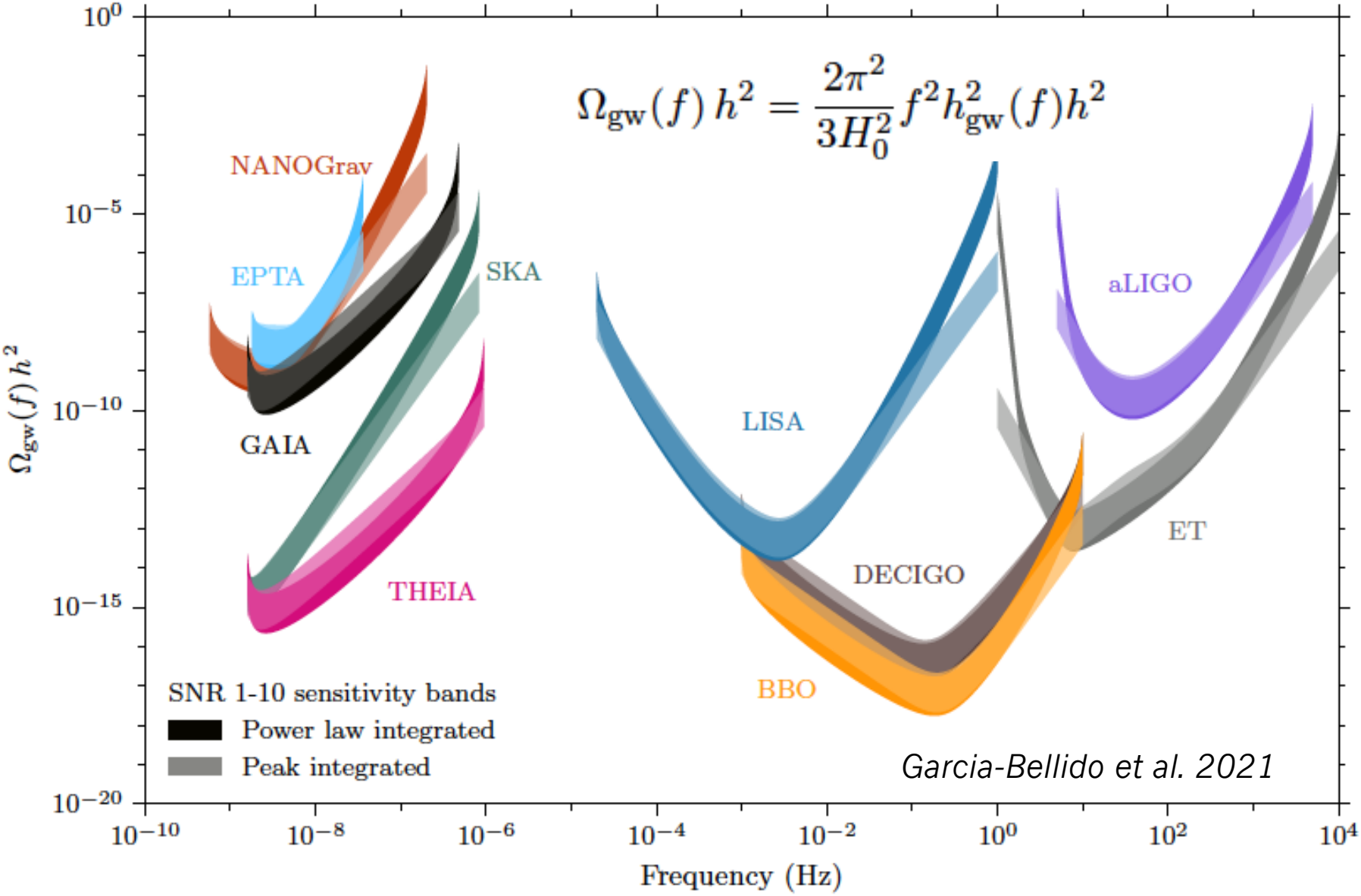

Garcia-Bellido et al. 2021

Take Home Comments

- Cross-correlating data between different observations:
  - PTAs
  - Astrometric missions: Gaia, Theia
- Advance Numerical Simulations Technique to Model Primordial Magnetic Fields and Turbulence
- Determine the mechanisms insuring the presence of viable magnetic field/turbulent sources in the early universe and correspondingly correct initial conditions:
  - Primordial magnetogenesis
  - Bubble collisions/nucleation – more realistic models
  - Sound waves as a source for turbulence
  - Axions driven turbulence and axion like particles driven inflation
  - Chiral sources and gravitational waves polarization

Thank you!

Questions?

Gravitational Waves Polarization

- If the parity in the early universe is violated – relic gravitational waves are polarized.
- The standard model predicts un-polarized gravitational waves

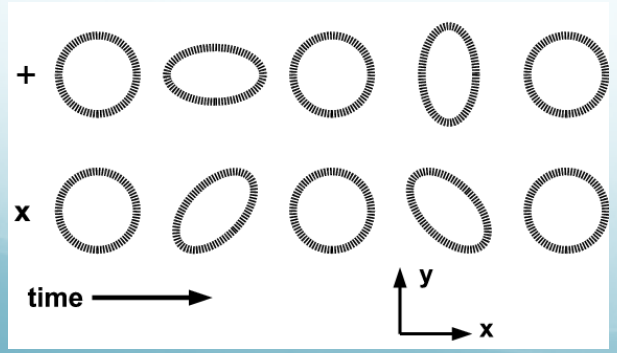

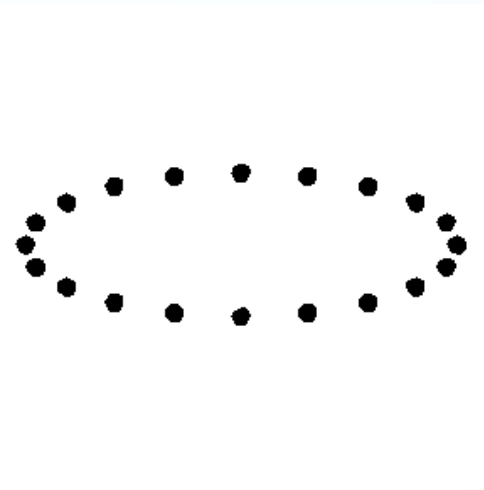

Linearly polarized + and X

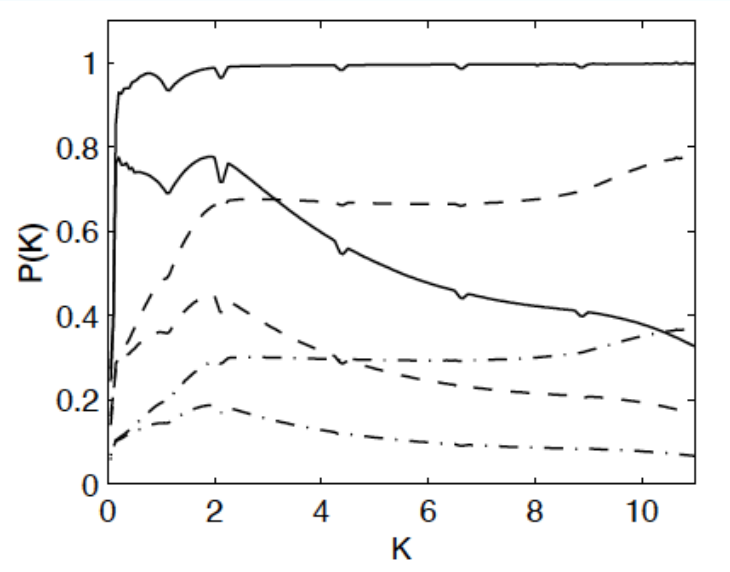

Kahniashvili, et al. 2005

$$\mathcal{P}(k) = \frac{\langle h^{+\star}(\mathbf{k})h^{+}(\mathbf{k}') - h^{-\star}(\mathbf{k})h^{-}(\mathbf{k}')\rangle}{\langle h^{+\star}(\mathbf{k})h^{+}(\mathbf{k}') + h^{-\star}(\mathbf{k})h^{-}(\mathbf{k}')\rangle} = \frac{\mathcal{H}(k)}{H(k)}.$$

- Assuming *stationary Kolmogoroff like turbulence* (HK) or *stationary helical Kolmogoroff turbulence* (HT)

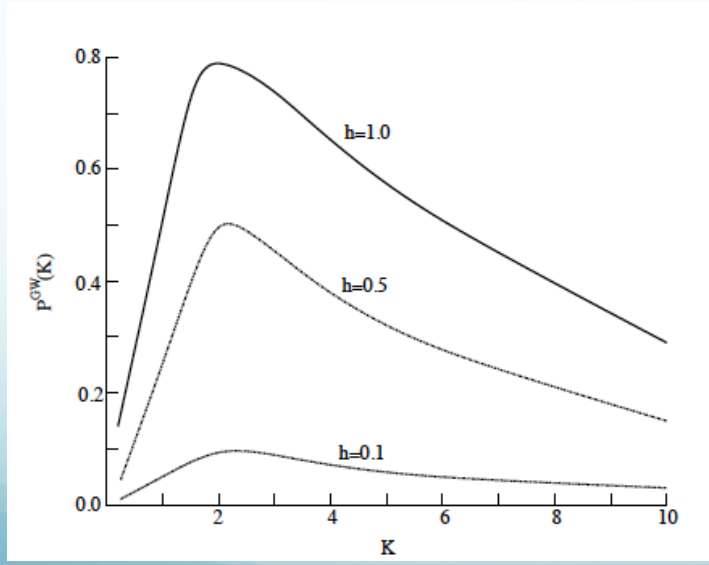

Kisslinger and Kahniashvili 2015

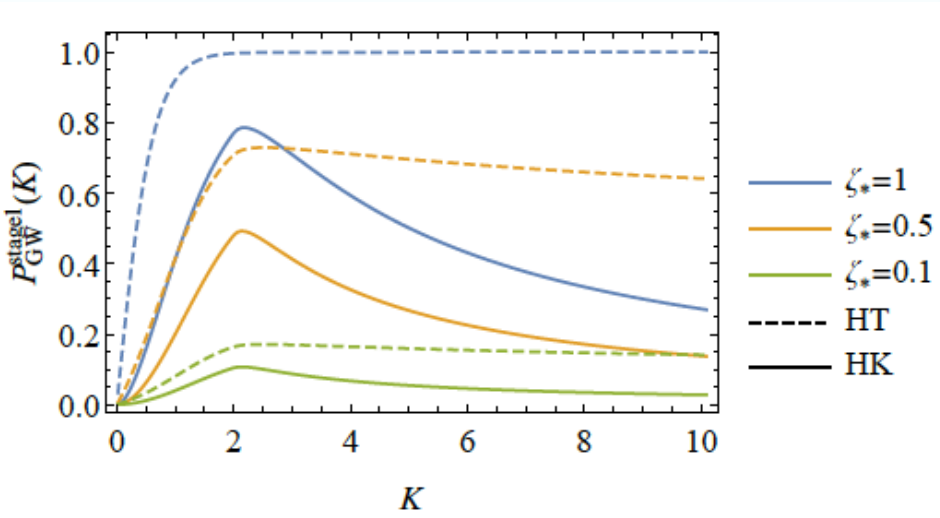

Figure 3: *The degree of polarisation of Stage 1 direct cascade GWs as a function of the normalised wavenumber $K = k/k_0$, assuming the indicated values of the helicity dissipation parameter h. The value of h coincides with the initial magnetic helicity fraction ζ_* for the helical Kolmogorov turbulence (HK) model as considered in this paper, shown by solid lines. We also show with dashed lines the polarisation fraction for Stage 1 turbulence driven by the Helicity Transfer (HT) model whose use may be more appropriate in the large helicity regime. However, we find the choice of Stage 1 model has no material impact on our overall results in this scenario as discussed in the text.*

Ellis et al. 2020

polarization spectrum

- Polarization spectrum retains information on parity violation at large wavelengths
  - Inverse cascading?

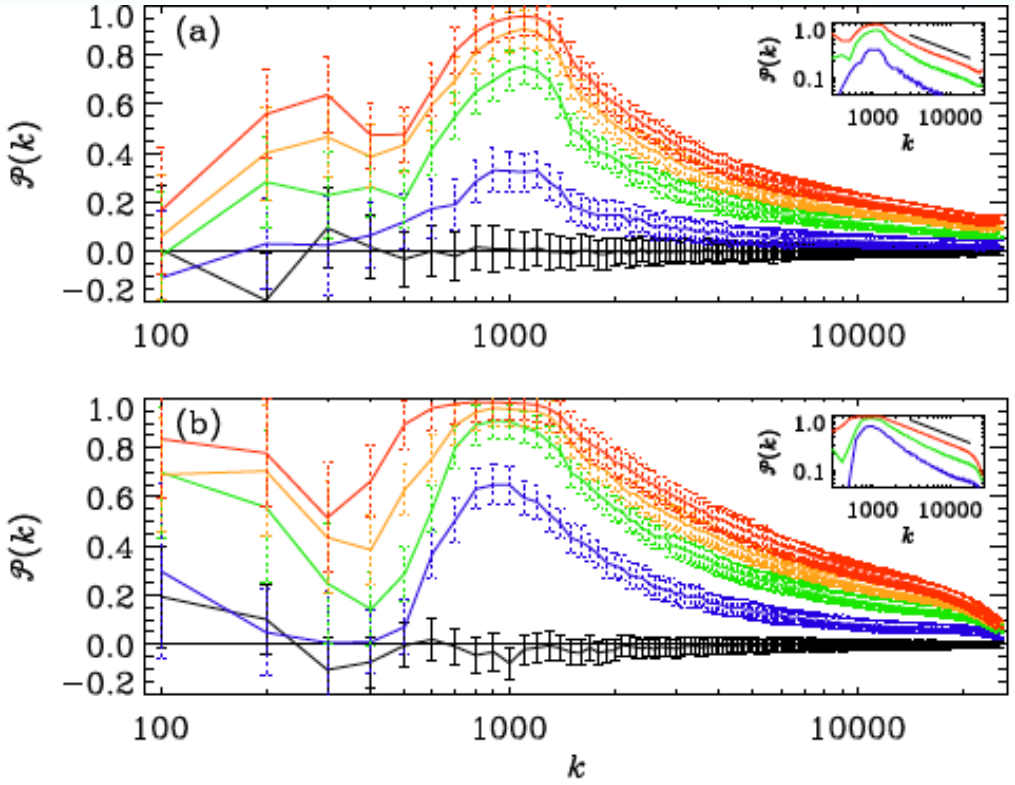

$$\mathcal{P}(k) = \frac{\langle h_+^\star(\mathbf{k})h_+(\mathbf{k}') - h_-^\star(\mathbf{k})h_-(\mathbf{k}')\rangle}{\langle h_+^\star(\mathbf{k})h_+(\mathbf{k}') + h_-^\star(\mathbf{k})h_-(\mathbf{k}')\rangle} = \frac{\mathcal{H}(k)}{H(k)}.$$

FIG. 3: Degree of circular polarization for (a) kinetically and (b) magnetically forced cases with $\sigma = 0$ (black) 0.1 (blue), 0.3 (green), 0.5 (orange), and 1 (red). Approximate error bars based on the temporal fluctuations and statistical spread for different random seeds of the forcing are shown as solid black lines for $\sigma = 0$ and as dotted lines otherwise.

Kahniashvili et al. 2020

more about polarization

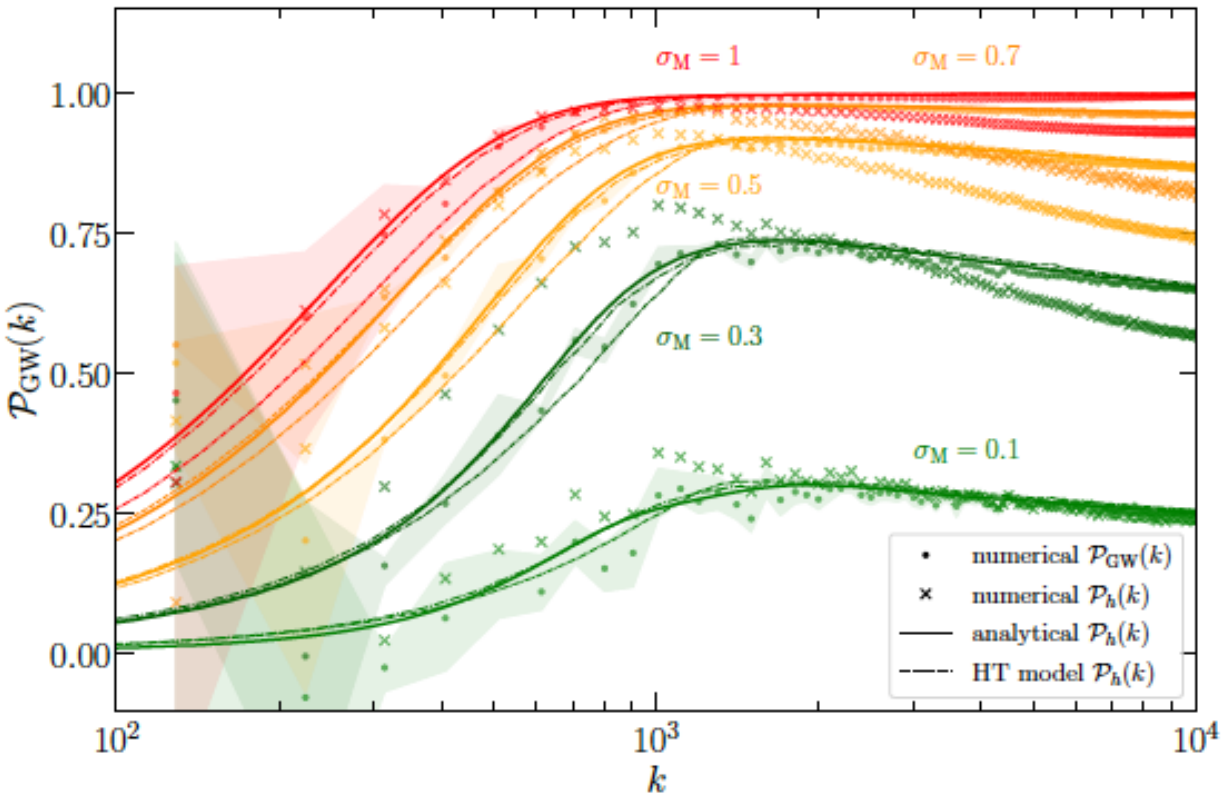

Roper Pol et al 2021

Figure 8. Polarization spectra $\mathcal{P}_{GW}(k)$ (dots) and $\mathcal{P}_h(k)$ (crosses) obtained from the numerical simulations for different σ_M, compared to $\mathcal{P}_h(k)$ computed from the analytical model (single power law and extended to a broken power law; see figure 7) using HT type of turbulence (dashed lines), and from the analytical integrals; see equations (3.2) and (3.3), using the numerical spectra of the turbulence (solid lines). Similar to figure 6, the shaded regions denote the maximum and minimum polarizations $\mathcal{P}_{GW}(k)$ of the fluctuations.

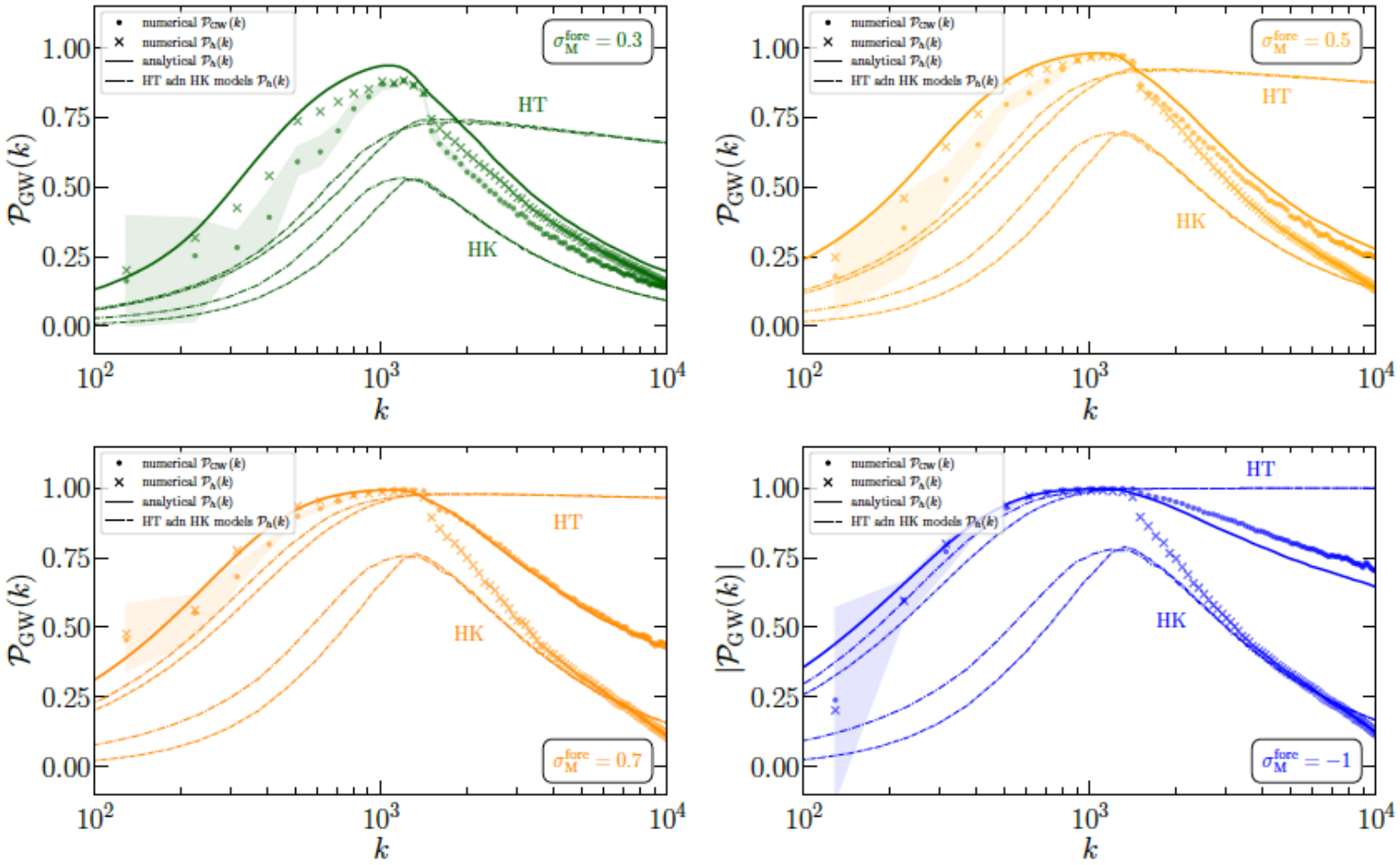

Figure 9. Similar to figure 8, polarization spectra $\mathcal{P}_{\rm GW}(k)$ and $\mathcal{P}_h(k)$ obtained from the numerical simulations for different σ, compared to $\mathcal{P}_h(k)$ obtained from the analytical model using both HK and HT types of turbulence (dashed lines; see figure 7), and obtained from the analytical integral, using the numerical spectrum of the turbulence (solid lines).

Roper Pol et al 2021

detection prospects

Measuring the net circular polarization of the stochastic gravitational wave background with interferometers

Valerie Domcke [a], Juan García-Bellido [b], Marco Peloso [c,d], Mauro Pieroni [b,e], Angelo Ricciardone [c], Lorenzo Sorbo [f], Gianmassimo Tasinato [g]

Abstract

Parity violating interactions in the early Universe can source a stochastic gravitational wave background (SGWB) with a net circular polarization. In this paper, we study possible ways to search for circular polarization of the SGWB with interferometers. Planar detectors are unable to measure the net circular polarization of an isotropic SGWB. We discuss the possibility of using the dipolar anisotropy kinematically induced by the motion of the solar system with respect to the cosmic reference frame to measure the net circular polarization of the SGWB with planar detectors. We apply this approach to LISA, re-assessing previous analyses by means of a more detailed computation and using the most recent instrument specifications, and to the Einstein Telescope (ET), estimating for the first time its sensitivity to circular polarization. We find that both LISA and ET, despite operating at different frequencies, could detect net circular polarization with a signal-to-noise ratio of order one in a SGWB with amplitude $h^2\Omega_{\rm GW} \simeq 10^{-11}$. We also investigate the case of a network of ground based detectors. We present fully analytical, covariant formulas for the detector overlap functions in the presence of circular polarization. Our formulas do not rely on particular choices of reference frame, and can be applied to interferometers with arbitrary angles among their arms.

arXiv:1910.08052 [astro-ph.CO]

- ✓ Dipolar anisotropy introduced by our proper motion, *Seto 2006* (for LISA and ET)
- ✓ Curvature of the Earth for ground based detectors, Seto & Taruya 2007, 2008

Domske et al. 2019:

In the present work we reconsider previous results by taking into account the full response functions and noise curves in the entire frequency band (for planar detectors). Moreover, we provide fully analytical and covariant expressions for the (parity-sensitive) response functions of a ground-based detector network.

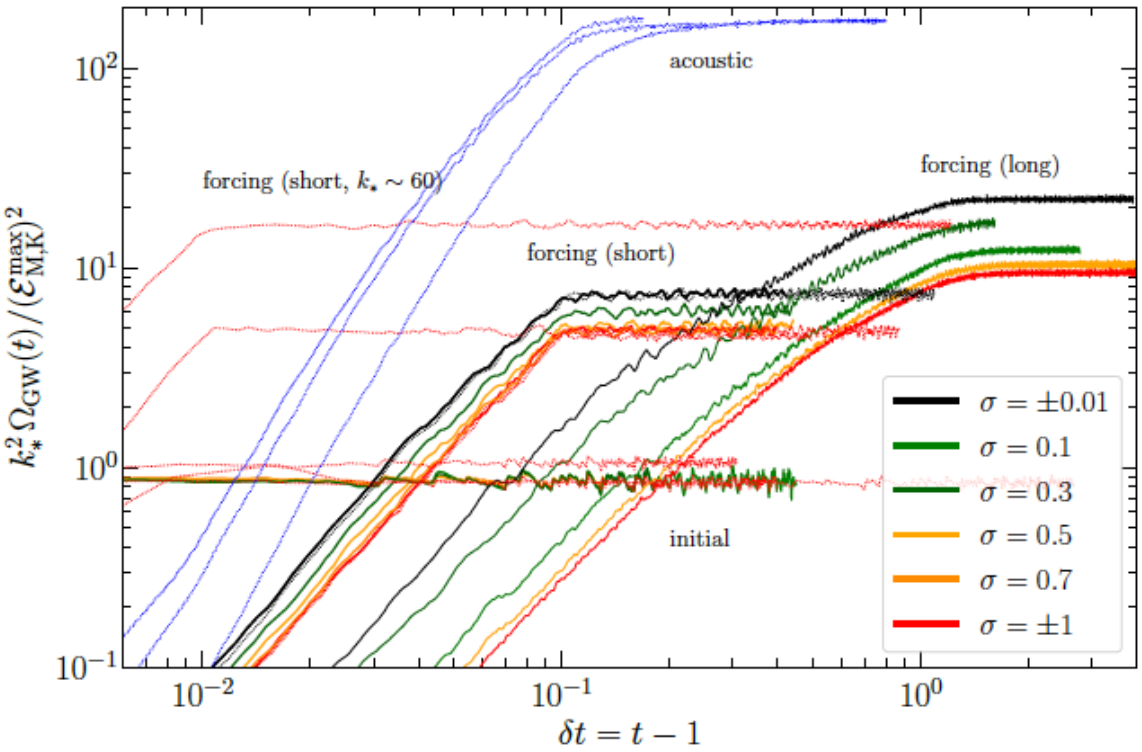

Figure 10. GW energy density $\Omega_{\rm GW}(t)$ in units of $a^{-4}(H_*/H_0)^2 = 1.644 \times 10^{-5}\,(g_*/100)^{-1/3}$; see equations (2.15) and (4.1), and compensated by $(\mathcal{E}_i^{\rm max})^2/k_*^2$, for i = M (magnetic) and K (kinetic), for the runs with an initial given magnetic field ('initial'), and for the runs with a forced magnetic field ('forcing (short)'), with $t_{\rm max} = 1.1$. Added for comparison are the runs in ref. [65] ('forcing (long)'), in which the magnetic field is forced for longer times ($t_{\rm max} = 3$), and the runs of ref. [81], which contain cases with initial given magnetic field, with forced magnetic field at $k_* = 60$, 600, and 6000, and runs of acoustic turbulence ('acoustic').

Roper Pol et al 2021